*Molecular Physics*
Vol. 106, No. 14, 20 July 2008, 1793–1801

Taylor & Francis
Taylor & Francis Group

RESEARCH ARTICLE

# High-resolution spectroscopy of the triple-substituted isotopologue of water molecule $D_2^{18}O$: the first triad

H.-Y. Ni[a], A.-W. Liu[a], K.-F. Song[a], S.-M. Hu[a]*, O.V. Naumenko[b], T.V. Kruglova[b] and S.A. Tashkun[b]

[a]*Hefei National Laboratory for Physical Sciences at Microscale, University of Science and Technology of China, Hefei, China;* [b]*Institute of Atmospheric Optics, Russian Academy of Sciences, Tomsk, Russia*

(*Received 30 April 2008; final version received 20 June 2008*)

The high-resolution Fourier-transform absorption spectrum of the triple-substituted isotopologue of the water molecule, $D_2^{18}O$ is measured in the 1700–9000 $cm^{-1}$ region. The transitions of the $\nu_1$, $2\nu_2$ and $\nu_3$ bands are assigned with the help of the high accuracy variational calculations based on an empirical mass-dependent Partridge–Schwenke potential energy surface. The fittings based on an effective Hamiltonian model are also utilized to confirm the assignments. A set of 816 precise ro-vibrational energy levels for the first triad of interacting vibrational states: (0 0 1), (1 0 0) and (0 2 0) is retrieved. With the upper state combination differences, the ground state energy levels are extended to $J^{max} = 23$ and $K_a^{max} = 13$. These levels can be used to check the quality of the recently available high accuracy *ab initio* potential energy surface of the water molecule.

**Keywords:** high-resolution spectroscopy; water molecule; $D_2O$; ro-vibrational energy levels; potential energy surface

## 1. Introduction

The water molecule is the one of the most extensively studied and simplest polyatomic molecules [1]. But the complicated spectrum of the water molecule is still far from being fully understood. The global modelling of the spectrum has to be based on the variational solution of the nuclear motions [2–4] instead of the traditional methods based on perturbation theory. Therefore the quality of the variation method relies on the accuracy of the potential energy surface (PES). Up to now one of the most accurate PESs is an empirical mass-dependent surface by Partridge and Schwenke [3]. It was frequently used to assign newly observed rovibrational transitions of the water isotopologues (see, for example, [5]). On the other hand, the calculation based on a pure *ab initio* PES [6] can reproduce about 18,000 vibration–rotation energy levels of five isotopologues ($H_2^{16}O$, $H_2^{18}O$, $H_2^{17}O$, $HD^{16}O$, $D_2^{16}O$) of water up to $J = 20$ with accuracy better than 1 $cm^{-1}$ on average.

An interesting question arises as to what extent the Born–Oppenheimer (B–O) approximation can be held when the same PES is applied to different isotopologues of water [7,8]. However, some studies of $HD^{16}O$ show strong non-Born–Oppenheimer effects [9,10]. The adiabatic and nonadiabatic corrections to the B–O approximation should be included in the study of the water molecule. It requires a comprehensive consideration of non-Born–Oppenheimer effects. Recently, the so-called CVRQD *ab initio* electronic ground-state adiabatic PES [11] resulting from the most accurate *ab initio* PES [6], has led to the most accurate equilibrium structure for all isotopologues of water [12] and an improved dipole moment surface [13]. Alternatively, new spectroscopically determined PESs are reported for $HD^{16}O$ up to 25,000 $cm^{-1}$ [14] and for $D_2^{16}O$ up to 16,000 $cm^{-1}$ [15]. We have recently undertaken the systematical study of a $^{18}O$ enriched water sample spectrum in the 1400–9336 $cm^{-1}$ region [16–18], resulting in new data on nine vibrational states of the $HD^{18}O$ molecule.

The triple-substituted isotopologue of water, $D_2^{18}O$, is of particular interest for testing the available PESs including the most accurate *ab initio* one to date [11]. Due to minor isotopologue abundance, the available spectroscopic data on $D_2^{18}O$ are still quite limited. To the best of our knowledge, there are just a few strong bands studied. The $\nu_2$ band of $D_2^{18}O$ was studied by Toth [19,20] and Wang *et al.* [21]. The $\nu_3$ and $\nu_2 + \nu_3$ bands were recently presented in [22]. The purpose of this work is to extend the spectroscopic investigations of the triple-substituted isotopologue of the water molecule, which could be applied to compare with the

*Corresponding author. Email: smhu@ustc.edu.cn

ISSN 0026–8976 print/ISSN 1362–3028 online

DOI: 10.1080/00268970802294067
http://www.informaworld.com

Table 1. Experimental conditions of the Fourier-transform absorption spectra recorded with enriched $D_2^{18}O$ sample.

| Filter/$cm^{-1}$ | Source | Beam splitter | Detector | Temperature/K | Path length/m | Pressure/Pa | Resolution/$cm^{-1}$ |
|---|---|---|---|---|---|---|---|
| 1700–2100 | Globar | KBr | InSb | 298.1 | 105 | 1935 | 0.005 |
| 1700–2100 | Globar | KBr | InSb | 298.8 | 15 | 1935 | 0.005 |
| 1700–2100 | Globar | KBr | InSb | 296.6 | 15 | 477 | 0.005 |
| 1700–2100 | Globar | KBr | InSb | 297.8 | 15 | 55 | 0.005 |
| 2000–2400 | Globar | KBr | InSb | 298.7 | 87 | 1935 | 0.006 |
| 2000–2400 | Globar | KBr | InSb | 298.9 | 15 | 1935 | 0.006 |
| 2000–2400 | Globar | KBr | InSb | 297.5 | 15 | 477 | 0.006 |
| 2000–2400 | Globar | KBr | InSb | 298.8 | 15 | 55 | 0.005 |
| 2550–3250 | Tungstem | $CaF_2$ | InSb | 298.7 | 105 | 1935 | 0.008 |
| 2550–3250 | Tungsten | $CaF_2$ | InSb | 297.8 | 15 | 1935 | 0.008 |
| 2550–3250 | Tungsten | $CaF_2$ | InSb | 296.1 | 15 | 477 | 0.007 |
| 2550–3250 | Tungsten | $CaF_2$ | InSb | 298.3 | 15 | 55 | 0.007 |
| 3300–4300 | Tungsten | $CaF_2$ | InSb | 296.5 | 105 | 1935 | 0.008 |
| 3300–4300 | Tungsten | $CaF_2$ | InSb | 296.5 | 15 | 1935 | 0.008 |
| 3300–4300 | Tungsten | $CaF_2$ | InSb | 296.2 | 15 | 477 | 0.009 |
| 3300–4300 | Tungsten | $CaF_2$ | InSb | 297 | 15 | 55 | 0.009 |
| 4100–5000 | Tungsten | $CaF_2$ | InSb | 297.5 | 105 | 1935 | 0.01 |
| 4100–5000 | Tungsten | $CaF_2$ | InSb | 295.8 | 15 | 477 | 0.011 |
| 4100–5000 | Tungsten | $CaF_2$ | InSb | 296.5 | 15 | 55 | 0.011 |
| | Tungsten | $CaF_2$ | InSb | 297.3 | 105 | 1935 | 0.015 |
| | Tungsten | $CaF_2$ | Ge | 297.3 | 105 | 1935 | 0.015 |
| | Tungsten | $CaF_2$ | Ge | 297.8 | 15 | 1935 | 0.015 |
| | Tungsten | $CaF_2$ | Ge | 295.6 | 15 | 477 | 0.015 |
| | Tungsten | $CaF_2$ | Ge | 297.3 | 15 | 55 | 0.015 |
| 5000–6300 | Tungsten | $CaF_2$ | InSb | 296.9 | 105 | 1935 | 0.015 |
| | Tungsten | $CaF_2$ | InSb | 298.2 | 15 | 55 | 0.013 |
| | Tungsten | $CaF_2$ | InSb | 296.1 | 15 | 477 | 0.013 |
| 1500–8000 | Tungsten | $CaF_2$ | InSb | 297.3 | 105 | 1935 | 0.015 |
| 5000–9000 | Tungsten | $CaF_2$ | Ge | 297.3 | 105 | 1935 | 0.015 |
| | Tungsten | $CaF_2$ | Ge | 297.8 | 15 | 1935 | 0.015 |
| | Tungsten | $CaF_2$ | Ge | 295.6 | 15 | 477 | 0.015 |
| | Tungsten | $CaF_2$ | Ge | 297.3 | 15 | 55 | 0.015 |

result derived from the variational calculations utilizing the *ab initio* PES. As will be seen from the forthcoming analysis, the high quality of the observed spectrum combined with the high accuracy variational calculations used for spectrum assignment, resulted in a large set of new energy levels for the (001), (100), and (020) vibrational states of $D_2^{18}O$. In addition, more high $J$ and $K_a$ energy levels in the (000) ground state were obtained. Both the variation calculations based on *ab initio* PES and effective Hamiltonian modelling will be applied to investigate these ro-vibrational energy levels quantitatively.

## 2. Experimental details

The enriched $D_2^{18}O$ water sample was purchased from ICON Services. The stated isotopic concentrations of $^{18}O$ is 98%. All spectra were recorded with a Fourier-transform spectrometer (Bruker IFS 120HR) equipped with a path length adjustable multi-pass gas cell. The cell was operating at room temperature. The sample pressure was measured by two capacitance manometers (MKS Baratron 627B) of 1 torr and 20 torr full-scale ranges with an overall accuracy of 0.15%. Because of the large variation of the absorption line intensities, different experimental conditions were applied in the measurements as listed in Table 1. The studied spectral region covers from 1700 to 9000 $cm^{-1}$. The line positions were calibrated by referring to known $H_2^{16}O$ and $HD^{16}O$ lines given by Toth [23]. The accuracy of the line positions of unblended and not-very-weak lines was estimated to be better than $4 \times 10^{-4}$ $cm^{-1}$. Part of the recorded spectrum around 2700 $cm^{-1}$ together with the assignments are presented in Figure 1.

Because we could not substitute the water adsorbed on the walls of the sample cell with the very limited amount of sample, it is difficult to precisely determine the isotopic composition of the sample used in our measurements. As discussed in [16], the isotope abundance of $D_2^{18}O$ in each spectrum was estimated

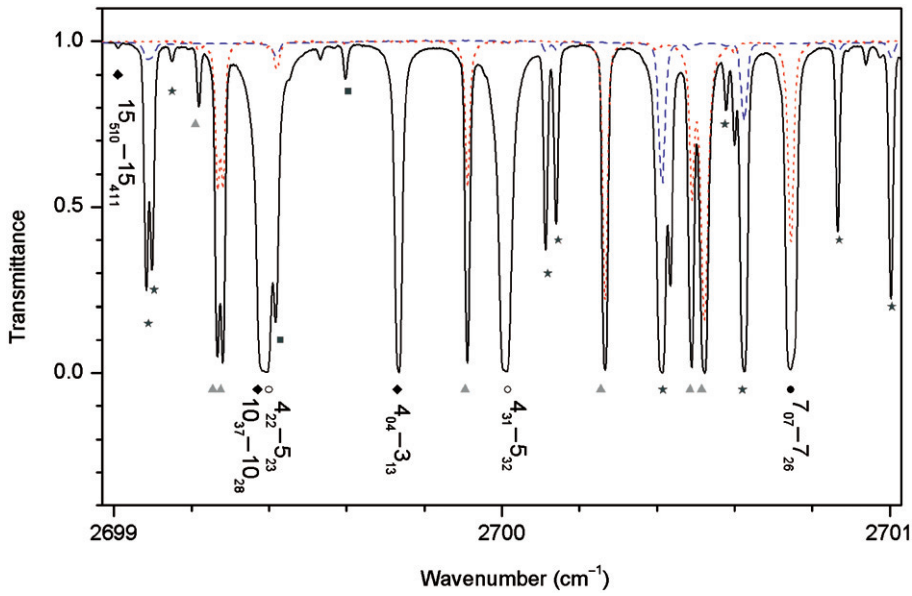


Figure 1. A small part of spectra of enriched $D_2^{18}O$ (black solid line), $H_2^{18}O$ (red dot line), and $D_2^{16}O$ (blue dash line) samples. Experimental conditions: absorption path length and sample pressure: 15 m and 477 Pa ($D_2^{18}O$), 15 m and 1307 Pa ($H_2^{18}O$), and 10 cm and 42 Pa ($D_2^{16}O$). The lines assigned to the $\nu_1$ and $\nu_3$ bands of $D_2^{18}O$ are marked by diamonds and hollow circles, respectively. The lines marked by solid circles are superimposed by $HD^{18}O$. Lines marked with triangles, asterisks and squares are due to $HD^{18}O$, $D_2^{16}O$ and $HD^{16}O$ lines, respectively.

by the comparison of the line intensities (retrieved from line profile fittings to our spectrum) of some 'moderate' lines with their values given in [22]. Then the isotopic abundance value derived in such a manner was used to determine the intensities of other lines, and to construct the line list for each spectrum.

## 3. Spectrum analysis and results

### 3.1. *Absorption lines attribution and line list construction*

Due to the D–H and $^{18}O$–$^{16}O$ exchange between the $D_2^{18}O$ sample and the water adsorbed in the walls of the sample cell, the observed spectra contain features of $HD^{18}O$, $H_2^{18}O$, $D_2^{16}O$, $HD^{16}O$ and $H_2^{16}O$, and some $CO_2$ and $N_2O$ lines as well due to the residual air in the interference chamber and the adsorbates on the walls of the sample cell. The isotope composition of the sample is illustrated in Figure 1. The resulting line list consisted of about 14,300 lines, which made the spectrum assignment very difficult. Moreover, many $D_2^{18}O$ lines overlap with the impurity transitions. Before the assignment, we cleaned the observed line list from impurity features using available literature data. $CO_2$, $N_2O$, $H_2^{16}O$ and $HD^{16}O$ lines could be easily removed from the line list using the HITRAN-2004 database [24]. The $H_2^{18}O$ and $HD^{18}O$ transitions were also identified with the help of our previous work [16]. Data from [20] were used to find the $D_2^{16}O$ lines.

However, there are still a lot of $HD^{16}O$, $HD^{18}O$, and $D_2^{16}O$ lines which have not been included in the literature but appear in our spectra. In this case, we compare the spectra recorded with samples of different isotopic composition. The relative line intensities from such different spectra will help to assign the lines to different isotopologues. For illustration, Figure 1 shows parts of the spectra recorded with $D_2^{18}O$ (solid line), $H_2^{18}O$ (dot line) and $D_2^{16}O$ (dash line) samples.

Since the above procedure becomes less reliable for weak and blended lines, we used the high accuracy variational calculations [14,15,25,26], and our computer code [27] for automatic assignment to confirm and extend our identifications for all water isotopologues, other than $D_2^{18}O$, which contributed to the observed spectrum. The absorption lines, which were left unassigned after performing the identification procedure, were preliminary attributed to $D_2^{18}O$ molecule, and included in the line list for further analysis.

### 3.2. *$D_2^{18}O$ spectrum assignment*

Assignment of $D_2^{18}O$ spectra was made with the help of a calculated line list of the water molecule. The list is based on a mass dependent PES $V^{\text{mass}}$ by Partridge and

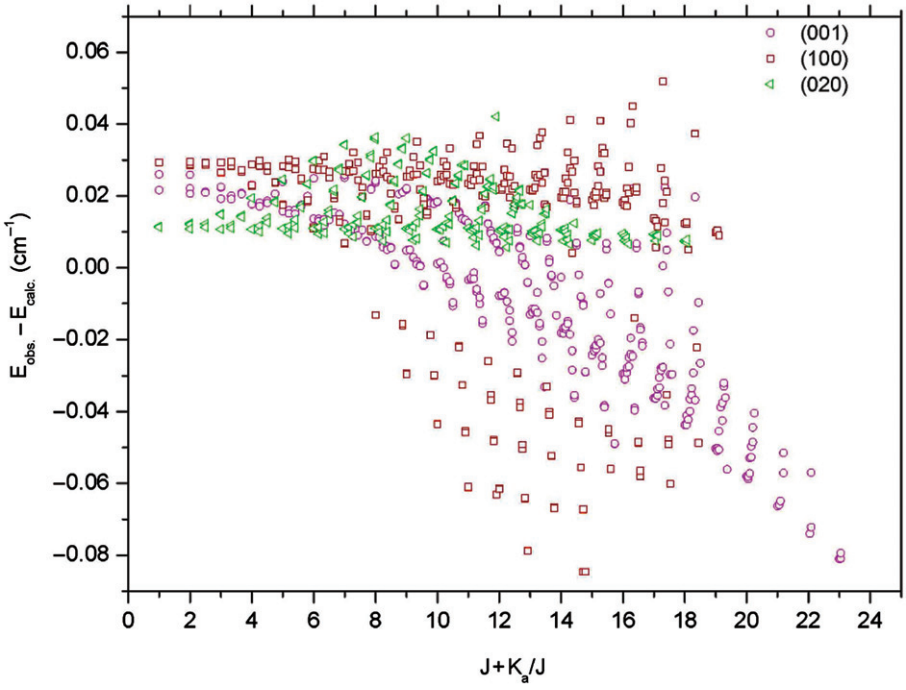


Figure 2. The difference between the experimental and variationally calculated energy values versus the quantity $(J + K_a/J)$ of the (001), (020), and (100) vibrational states of $D_2^{18}O$.

Schwenke [3] and an *ab initio* dipole moment surface by Schwenke and Partridge [28]. Details of construction and discussion of the $V^{mass}$ accuracy can be found in [3]. In the case of $D_2^{16}O$, the line list performs well for lower lying levels but deteriorates rapidly for highly excited states. It has been shown that for the $D_2^{16}O$ line positions in the 8800–9520 $cm^{-1}$ region, the differences between the observed and calculated values reach up to 1.5 $cm^{-1}$ [29]. Moreover, the standard spectroscopic assignment $(v_1, v_2, v_3, K_a, K_c)$ of the calculated energy levels becomes ambiguous and erroneous for highly excited states. The same problems can be expected for the variational calculations involving the $D_2^{18}O$ molecule.

In order to improve the convergence of the highly excited energies in the $D_2^{18}O$ line list, the maximal size of the final Hamiltonian matrices in the calculations was set to 15,000. In [3] the size was 7500. All other input parameters of calculations were kept the same as in [3]. The line list was calculated with the VTET computer code given by Schwenke [30,31], assuming for pure $D_2^{18}O$, reference temperature 296 K, intensity cutoff $10^{-27}$ cm per molecule and $J_{max} = 30$. The list is available online [26].

The assignment process has confirmed the high quality of the theoretical line list. The maximum *obs.–calc.* deviation of the line positions is 0.08 $cm^{-1}$ in absolute value for all assigned lines, while the *rms* deviation is 0.025 $cm^{-1}$. Figure 2 illustrates the *obs.–calc.* deviations as a function of the rotational quantum numbers $J + K_a/J$ for all observed energy levels. It is clear that the *obs.–calc.* deviations vary smoothly with the increasing $J + K_a/J$, which helped very much in the assignment process. The *obs.–calc.* deviations for $K_a \geq 7$ energy levels of the (100) state become systematically negative, as shown on Figure 2.

The agreement between the observed and calculated line intensities represents another important criterion in the assignment process. Figure 3 shows the comparison of the observed (upper panel) and calculated (lower panel) line intensities. It is clear that the calculated and observed intensities agree well enough for the unambiguous line assignment. We also compared the predicted variational intensities for the $v_3$ transitions with the experimental data given in [22], and obtained very good agreement with the averaged $I_{obs.}/I_{calc.}$ ratio of 0.98.

However, despite the high accuracy of variational calculations, the high density of the observed lines prevented us from assigning the weak $D_2^{18}O$ transitions which could not be confirmed with the ground state combination differences (GSCD). The distance between adjacent observed lines is very often less than the possible error in the variationally calculated line position. In this case, we performed the energy levels modelling under the effective Hamiltonian (EH)

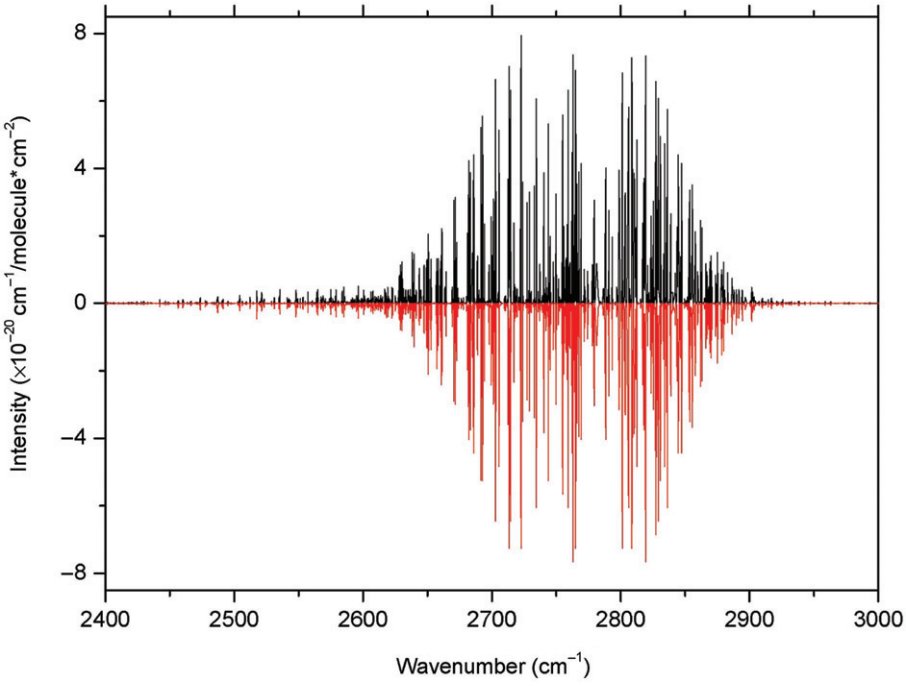


Figure 3. The comparison of the observed (upper panel) and *ab initio* calculated (lower panel) line intensities of $D_2^{18}O$.

approach, which is known to provide the best accuracy of the energy levels reproduction, at least for low lying vibrational states (see next section). High accuracy calculations of the $D_2^{18}O$ transitions within the EH approach not only confirmed the majority of the assignments based on variational calculations, but also allowed us to extend the assignments on those transitions with very high $J/K_a$ values. The comparisons of the available $D_2^{18}O$ lines [22], our experimental data, and variational calculations are given in Figure 4. Obviously, the data given in [22] are limited to the strongest observed lines only.

The resulting line list which contains 3529 assigned absorption lines of the $D_2^{18}O$ molecule are given in Supplementary Material I (available via the multimedia link on the online article webpage). This list incorporates observed line positions and intensities, followed by the calculated intensities and rovibrational assignment. Note that due to the difficulties discussed in the experimental section, the given 'experimental' line intensities can be only considered as quick reference. We leave in the final line list a number of $D_2^{18}O$ lines superimposed to other water isotopologues or $CO_2$ lines, if the contribution from $D_2^{18}O$ is considered more than 20%. Including the multiple assignments attached to the same blended experimental line, the resulting list consists of 3879 transitions in total. A number of transitions from the (010) state to the (011), (110), and (030) upper states were assigned in the spectrum using our data on the (011)–(000), (110)–(000) and (030)–(000) absorption bands in the 3300–4300 $cm^{-1}$ spectral region which will be presented later elsewhere.

### 3.3. *The energy levels derivation*

The upper experimental energy levels were initially derived by adding the observed frequencies to the corresponding ground state experimental energies taken from [19]. However, many of our assigned transitions involve highly excited rotational energy levels of the lower vibrational state which are not available in [19]. We assigned the $D_2^{18}O$ absorption lines with upper $J$ and $K_a$ values as high as 23 and 13, while the corresponding values of the available ground state energy levels given in [19] are 16 and 9, respectively. But any fitting and/or extrapolation based on the available ground state energy levels could hardly provide us with new calculated high $J/K_a$ levels without a loss of accuracy.

From the assignment of the low $J$ and $K_a$ transitions in the $\nu_1$, $\nu_3$ and $2\nu_2$ bands, the ground states combination differences show that the accuracy of our experimental $D_2^{18}O$ line positions is about $2 \times 10^{-4}$ $cm^{-1}$. In this case, the combination differences which include transitions on the same upper level

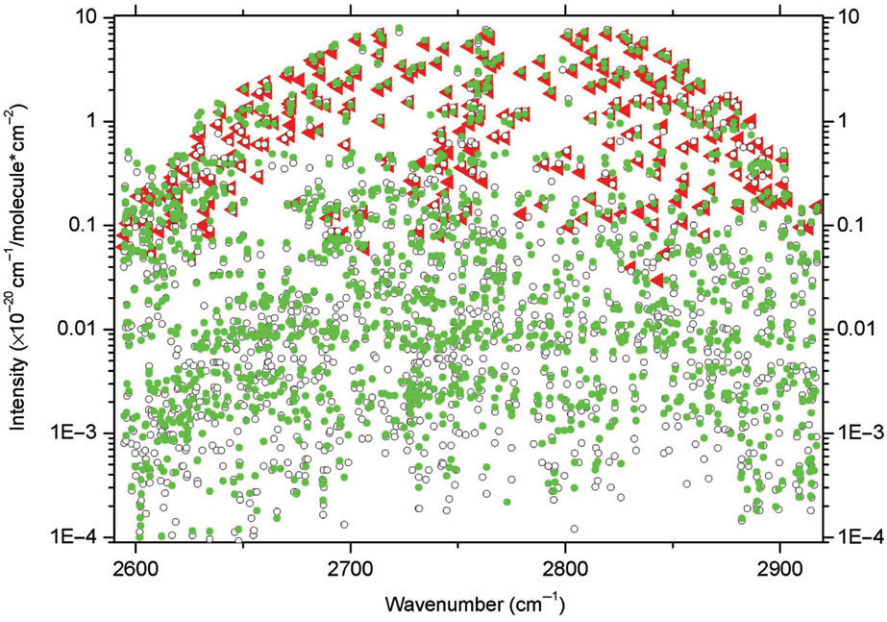


Figure 4. The comparison of the observed (solid green circle), *ab initio* calculated (hollow black circle) and Toth's [22] (red triangle) line intensities.

but from both known and unknown lower energy levels was used to determine the unknown ground state energy levels. The transitions originating from the same lower level also form a sort of combination differences of the upper energy levels. The (000) experimental energy levels were derived as an averaged value over all transitions involved in the combination differences. In this way we could extend considerably the experimental energy levels set for the ground state of the $D_2^{18}O$ molecule. This set was then modelled using a rotational Hamiltonian written through generating functions [32]. The initial set of the ground state parameters was derived by S.N. Mikhailenko through the fitting to the variational (000) ground state energy levels ($J \leq 24$) provided by the present study. These parameters were then partly refined through the fitting to the experimental (000) energy levels. The quality of the calculation proved to be very high, and, finally, in the case of poor combination difference, matching with the calculated (000) energy level served as the important criterion in the choice of one or another experimental value for the considered (000) level.

The experimental and EH calculated energy levels list of the (000) state of $D_2^{18}O$ molecule as well as the corresponding rotational and centrifugal distortion parameters which can reproduce experimental data within $0.00025\,cm^{-1}$ are given in Supplementary Material II (available via the multimedia link on the online article webpage). The accuracy of the (000) experimental energy levels derived here is estimated as $\pm 0.0003\,cm^{-1}$ on average. However, for $J \geq 16$ levels the experimental uncertainty may accumulate and reach up to $0.001–0.002\,cm^{-1}$ for some energy levels. In addition, our analysis shows that the deviations in some of the (000) energy levels derived from the far infrared study [19] reach up to $0.0166\,cm^{-1}$ (for instance, the [16 0 16], [16 1 16] energy levels). These energy levels with large deviations marked with 'IC' are replaced by the corresponding infrared data from the present work. The calculated energy levels set for the (000) state of $D_2^{18}O$ molecule was used in this study for the energy levels derivation of the (001), (100), and (020) vibrational states.

The upper energy levels set derived in this study is presented in Supplementary Material III (available via the multimedia link on the online article webpage). In total, 816 energy levels were derived for the (100), (001), and (020) vibrational states of the $D_2^{18}O$ molecule, while only 144 energy levels were previously reported in the literature [22] for the (001) vibrational state, including 17 levels (marked with 'd') corrected in this study. Note that the upper energy levels with high $J$ and $K_a$ derived in this study may include uncertainties far beyond the accuracy of the experimental line positions due to the accumulation of the errors in the corresponding ground state energy levels. We acknowledge that the values of these upper energy levels can be easily corrected using improved ground state levels (if available) and the attached list of the assignments.

Table 2. Spectroscopic parameters of the (001), (100) and (020) vibrational states of the $D_2{}^{18}O$ molecule (in $cm^{-1}$).

| | (001) | (100) | (020) |
|---|---|---|---|
| $E$ | 2767.499742(160) | 2660.792745(170) | 2320.721369(180) |
| $A$ | 14.5645502(330) | 14.8381580(380) | 17.7119139(520) |
| $B$ | 7.24421141(830) | 7.1856997(150) | 7.3959984(110) |
| $C$ | 4.7576801(270) | 4.7452662(280) | 4.70065751(900) |
| $\Delta_K \times 10^3$ | 8.10673(160) | 8.57452(230) | 20.83824(470) |
| $\Delta_{JK} \times 10^3$ | −1.481402(560) | −1.465810(870) | −2.32421(120) |
| $\Delta_J \times 10^4$ | 3.167094(390) | 3.054902(700) | 3.617985(600) |
| $\delta_K \times 10^4$ | 3.23657(590) | 2.87375(900) | 12.97035(740) |
| $\delta_J \times 10^4$ | 1.268926(210) | 1.212500(280) | 1.502281(340) |
| $H_K \times 10^5$ | 1.41943(340) | 1.56437(540) | 8.6529(170) |
| $H_{KJ} \times 10^6$ | −2.2487(200) | −2.0595(230) | −11.0005(520) |
| $H_{JK} \times 10^7$ | −2.8207(240) | −1.9093(290) | 9.801(100) |
| $H_J \times 10^8$ | 6.7083(110) | 6.3121(270) | 8.56760(820) |
| $h_K \times 10^6$ | 3.39854(660) | 3.70212(800) | 22.2595(420) |
| $h_{JK} \times 10^8$ | −7.5008(860) | −6.975(100) | −25.935(500) |
| $h_J \times 10^8$ | 3.36347(400) | 3.19752(460) | 4.25779(710) |
| $L_K \times 10^8$ | −3.9113(320) | −4.2707(560) | −46.811(290) |
| $L_{KJ} \times 10^8$ | 1.8420(290) | 1.6783(290) | 16.874(170) |
| $L_{KJK} \times 10^9$ | −3.9376(520) | −4.882(110) | −52.076(560) |
| $L_{JK} \times 10^{10}$ | 1.1372(300) | 0.3291(340) | −4.752(340) |
| $L_J \times 10^{11}$ | −1.7852(130) | −1.6555(320) | – |
| $l_K \times 10^8$ | −1.9624(100) | −2.2300(200) | −25.043(200) |
| $l_J \times 10^{12}$ | −9.2451 | −9.2451 | – |
| $P_K \times 10^{11}$ | 7.386(130) | 6.586(210) | 95.47(140) |
| $P_{KJ} \times 10^{11}$ | −5.196(170) | −3.253(150) | – |
| $P_{KJK} \times 10^{11}$ | 1.0904(460) | 1.4506(590) | −9.012(400) |
| $P_{JK} \times 10^{11}$ | – | – | 4.750(140) |
| $p_K \times 10^{11}$ | 4.1932 | 4.1932 | 39.628(860) |
| $p_{KJ} \times 10^{10}$ | – | – | 1.1906(340) |

Note: Values in parentheses are the $1\sigma$ statistical confidence intervals to the last digit. Parameters without confidence intervals were constrained by the corresponding values for the (000) state.

## 4. Modelling the experimental energy levels

Since the vibrational states (001), (100) and (020) which form the first triad of the $D_2^{18}O$ molecule are strongly interacting, we applied in the analysis the following Hamiltonian model,

$$H = \sum_{i,j=1}^{3} |i\rangle\langle j| H_{ij}, \tag{1}$$

where $|1\rangle = (001)$, $|2\rangle = (100)$ and $|3\rangle = (020)$.

The diagonal operators $H_{ii}$ $(i = 1, 2, 3)$ are the usual Watson's operators [33]:

$$\begin{aligned} H = {} & E + \left[A - \frac{1}{2}(B+C)\right] J_z^2 + \frac{1}{2}(B+C) J^2 \\ & - \Delta_K J_z^4 - \Delta_{JK} J_z^2 J^2 - \Delta_J J^4 \\ & + H_K J_z^6 + H_{KJ} J_z^4 J^2 + H_{JK} J_z^2 J^4 + H_J J^6 \\ & + L_K J_z^8 + L_{KJ} J_z^6 J^2 + L_{KJK} J_z^4 J^4 + L_{JK}^{v} J_z^2 J^6 + L_J J^8 \\ & + P_K J_z^{10} + P_{KJ} J_z^8 J^2 + P_{KJK} J_z^6 J^4 + P_{JK} J_z^4 J^6 + \cdots \\ & + \frac{1}{2}(B-C) J_{xy}^2 - \delta_K [J_z^2, J_{xy}^2]_+ - 2\delta_J J^2 J_{xy}^2 \\ & + h_K [J_z^4, J_{xy}^2]_+ + h_{JK} [J_z^2, J_{xy}^2]_+ J^2 + 2h_J J_{xy}^2 J^4 \\ & + l_K [J_z^6, J_{xy}^2]_+ + l_{KJ} [J_z^4, J_{xy}^2]_+ J^2 \\ & + l_{JK} [J_z^2, J_{xy}^2]_+ J^4 + 2l_J J_{xy}^2 J^6 \\ & + p_K [J_z^8, J_{xy}^2]_+ + p_{KJ} [J_z^6, J_{xy}^2]_+ J^2 + \cdots, \end{aligned} \tag{2}$$

where $J_{xy}^2 = J_x^2 - J_y^2$ and $[A, B]_+ = AB + BA$.

The nondiagonal parts $H_{ij}$ $(i \neq j)$ correspond to resonance interactions. $H_{12} = H_{21}^+$ and $H_{13} = H_{31}^+$ correspond to the Coriolis interactions,

$$\begin{aligned} H_{i1} = {} & {}^{i1}C_y (iJ_y) + {}^{i1}C_{yK} [iJ_y, J_z^2]_+ + {}^{i1}C_{yJ} (iJ_y) J^2 \\ & + {}^{i1}C_{yKK} [iJ_y, J_z^4]_+ + \cdots + {}^{i1}C_{xz} [J_x, J_z]_+ \\ & + {}^{i1}C_{xzK} [J_z^3, J_x]_+ + {}^{i1}C_{xzJ} [J_x, J_z]_+ J^2 \\ & + {}^{i1}C_{xzKJ} [J_x, J_z^3]_+ J^2 + {}^{i1}C_{xzJJ} [J_x, J_z]_+ J^4 + \cdots. \end{aligned} \tag{3}$$

$H_{23} = H_{32}^+$ is for the Fermi-type interaction,

$$\begin{aligned} H_{23} = {} & F_K J_z^2 + F_{xy} (J_x^2 - J_y^2) - F_{xyK} [J_z^2, (J_x^2 - J_y^2)]_+ \\ & - 2F_{xyJ} J^2 (J_x^2 - J_y^2) + \cdots. \end{aligned} \tag{4}$$

Observed energy levels were included step by step in the fitting, and it led to parameters refining and improvement of the calculation quality. The EH predictions were then used to confirm and extend the assignments. Of all 816 observed energy levels, 798 were included in the final fitting. The *rms* deviation of $0.0005\,cm^{-1}$ was achieved by using 76 diagonal and 12 resonance parameters, which are presented in Tables 2 and 3 together with 68% confidential intervals. Eighteen energy levels (about 2%) marked by '*' in Supplemental Material III were excluded from the fitting because they have large *obs.–calc.* deviations ($0.0025$–$0.0175\,cm^{-1}$), which are several times over the average value. The majority of these excluded energy levels were derived from weak or blended lines.

Table 3. Parameters of resonance interactions for the first triad (in $cm^{-1}$).

| Parameter | Value | Parameter | Value |
|---|---|---|---|
| $F_K^{100-020} \times 10^2$ | −7.5245(380) | $C_{xzk}^{100-001} \times 10^5$ | −8.902(500) |
| $F_J^{100-020} \times 10^2$ | −1.6194(100) | $C_{yk}^{100-001} \times 10^3$ | −1.6379(690) |
| $F_{xy}^{100-020} \times 10^3$ | 4.4951(690) | $C_y^{100-001} \times 10^1$ | 4.1079(320) |
| $F_{xyK}^{100-020} \times 10^5$ | −5.298(160) | $C_{xz}^{100-001} \times 10^1$ | −1.31960(170) |
| $C_{xzJ}^{100-001} \times 10^5$ | −2.074(110) | $C_{xzJ}^{020-001} \times 10^5$ | 6.6259(890) |
| $C_{xzKJ}^{020-001} \times 10^7$ | −1.7663(610) | $C_{xzJJ}^{020-001} \times 10^8$ | −5.262(170) |

Notes: *F* and *C* denote Fermi-type and Coriolis-type interactions respectively. Values in parentheses are the $1\sigma$ statistical confidence intervals to the last digit.

It has been found that the resonance interactions inside the first triad play an important role in the energy levels modelling. Figure 5 shows the average mixing coefficients of the wavefunctions. It can be found that the Coriolis-type resonance interactions between the (100) and (001) states appear at $J=5$ and grow rapidly up to about 9% at $J=11$. Starting from $J=12$ the Fermi-type resonance takes place between the (020) and (100) states causing divergence of the resonance curves for the (100) and (001) states which coincide up to $J=11$. Averaged resonance mixing for the first triad states amounts up to 15% for $J=23$. At the same time, the maximal mixing coefficients of the wavefunctions may reach up to 49% for the (100)–(001) interaction which leads to ambiguous ro-vibrational labelling.

## 5. Conclusion

High resolution Fourier transform absorption spectrum of the $D_2^{18}O$ enriched water sample was recorded in the 1700–9000 $cm^{-1}$ region. The transitions of the first triad were assigned using high accuracy variational and effective Hamiltonian calculations. A set of 816 precise energy levels were derived for the (100),

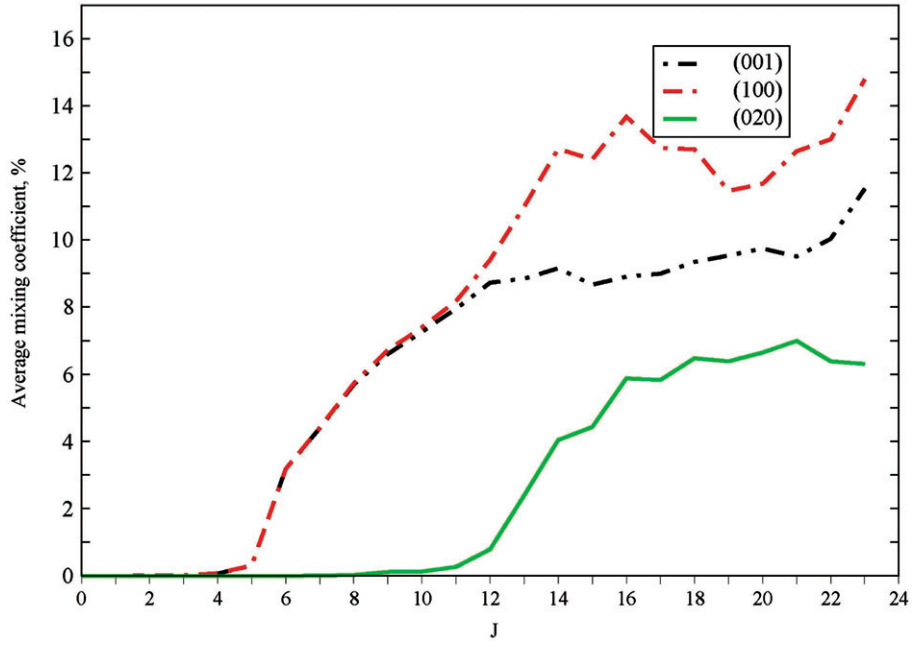


Figure 5. On-average mixing coefficients of the wavefunctions (see text) for a given *J* of the (001), (100), and (020) vibrational states of $D_2^{18}O$.

(001), and (020) states. A detailed identification list including 3879 transitions of $D_2^{18}O$ was generated in the analysed spectral region, while only 298 strong lines of the $\nu_3$ band were identified previously [22] in the 2594–2918 $cm^{-1}$ region. Rotational, centrifugal distortion, and resonance parameters of the Watson-type rotational Hamiltonian were derived by fitting the observed upper energy levels, which reproduce the initial data with the accuracy close to the experimental uncertainties. An extended and corrected set of the (0 0 0) ground state energy levels was also constructed using infrared transitions. The study on the higher overtones will be carried out in sequence. The obtained quantitative information will extend our knowledge about the energy levels structure of such triple-substituted isotopologues of the water molecule, and may be used for further optimization of the potential energy function of water.

## Acknowledgements

We thank Dr D.W. Schwenke for providing us with the VTET computer code for variational calculations. O.V.N. is grateful to Dr S.N. Mikhailenko for giving an opportunity to use his computer code for the molecular energy levels modelling in the frame of G-function approach, as well as for providing her with the initial parameters set for the (000) state of $D_2^{18}O$. The work is jointly supported by NSFC-China (50721091 & 10574124) and RFBR-Russia (N.06-03-39014), by Chinese Ministry of Science and Technology (2007CB815203), and by the Fok Ying Dong Education Foundation (101013).

## References

[1] P.F. Bernath, Phys. Chem. Chem. Phys. **4**, 1501 (2002).
[2] O.L. Polyansky, N.F. Zobov, S. Viti, *et al.*, Science **277**, 346 (1997).
[3] H. Partridge and D.W. Schwenke, J. Chem. Phys. **106**, 4618 (1997).
[4] O.L. Polyansky, J. Tennyson, and N.F. Zobov, Spectrochim. Acta, Part A **55**, 659 (1999).
[5] S.N. Mikhailenko, G.Ch. Mellau, E.N. Starikova, *et al.*, J. Mol. Spectrosc. **233**, 32 (2005).
[6] O.L. Polyansky, A.G. Császár, S.V. Shirin, *et al.*, Science **299**, 539 (2003).
[7] V.G. Tyuterev, S.A. Tashkun, P. Jensen, *et al.*, J. Mol. Spectrosc. **198**, 57 (1999).
[8] V.G. Tyuterev, S.A. Tashkun, and D.W. Schwenke, Chem. Phys. Lett. **348**, 223 (2001).
[9] N.F. Zobov, O.L. Polyansky, C.R. Le Sueur, *et al.*, Chem. Phys. Lett. **260**, 381 (1996).
[10] D.W. Schwenke, J. Phys. Chem. A **105**, 2352 (2001).
[11] P. Barletta, J. Tennyson, S.V. Shirin, *et al.*, J. Chem. Phys. **125**, 204307 (2006).
[12] A.G. Császár, G. Czakó, T. Furtenbacher, *et al.*, J. Chem. Phys. **122**, 214205 (2005).
[13] L. Lodi, R.N. Tolchenov, J. Tennyson, *et al.*, J. Chem. Phys. **128**, 044304 (2008).
[14] S.N. Yurchenko, B.A. Voronin, R.N. Tolchenov, *et al.*, J. Chem. Phys. **128**, 044312 (2008).
[15] S.V. Shirin, N.F. Zobov, and O.L. Polyansky, J. Quant. Spectrosc. Radiat. Transf. **109**, 549 (2008).
[16] A.-W. Liu, J.-H. Du, K.-F. Song, *et al.*, J. Mol. Spectrosc. **237**, 149 (2006).
[17] A.-W. Liu, O. Naumenko, K.-F. Song, *et al.*, J. Mol. Spectrosc. **236**, 127 (2006).
[18] A.-W. Liu, S.-M. Hu, C. Camy-Peyret, *et al.*, J. Mol. Spectrosc. **237**, 53 (2006).
[19] R.A. Toth, J. Mol. Spectrosc. **162**, 41 (1993).
[20] R.A. Toth, J. Mol. Spectrosc. **195**, 98 (1999).
[21] W.F. Wang, T.L. Tan, B.L. Tan, *et al.*, J. Mol. Spectrosc. **176**, 226 (1996).
[22] R.A. Toth, J. Mol. Struc. **742**, 49 (2005).
[23] R.A. Toth, line lists of water vapour parameters from 500–8000 $cm^{-1}$, see http://mark4sun.jpl.nasa.gov.data/spec/$H_2O$/
[24] L.S. Rothman, D. Jacquemart, A. Barbe, *et al.*, J. Quant. Spectrosc. Radiat. Transf. **96**, 139 (2005).
[25] S.V. Shirin, O.L. Polyansky, N.F. Zobov, *et al.*, J. Mol. Spectrosc. **236**, 216 (2006).
[26] http://spectra.iao.ru
[27] A.D. Bykov, O.V. Naumenko, A.M. Pshenichnikov, *et al.*, Opt. Spectrosc. **93**, 528 (2003).
[28] D.W. Schwenke and H. Partridge, J. Chem. Phys. **113**, 6592 (2000).
[29] O.V. Naumenko, O. Leshchishina, S. Shirin, *et al.*, J. Mol. Spectrosc. **238**, 79 (2006).
[30] D.W. Schwenke, J. Phys. Chem. **100**, 2867 (1996).
[31] D.W. Schwenke, J. Phys. Chem. **100**, 18884 (1996).
[32] Vl.G. Tyuterev, J. Mol. Spectrosc. **151**, 97 (1992).
[33] J.K.G. Waston, J. Chem. Phys. **46**, 1935 (1967).